

Article

# Analysis of the Influence of Compensation Capacitance Errors of a Wireless Power Transfer System with SS Topology

Yi Wang \*, Fei Lin, Zhongping Yang and Zhiyuan Liu

School of Electrical Engineering, Beijing Jiaotong University, Shangyuan Village No. 3, Haidian District, Beijing 100044, China; flin@bjtu.edu.cn (F.L.); zhpyang@bjtu.edu.cn (Z.Y.); 17126022@bjtu.edu.cn (Z.L.)

\* Correspondence: 16121534@bjtu.edu.cn; Tel.: +86-156-5293-7915

Received: 29 October 2017; Accepted: 14 December 2017; Published: 19 December 2017

**Abstract:** In this study, in order to determine the reasonable accuracy of the compensation capacitances satisfying the requirements on the output characteristics for a wireless power transfer (WPT) system, taking the series-series (SS) compensation structure as an example, the calculation formulas of the output characteristics, such as the power factor, output power, coil transfer efficiency, and capacitors' voltage stress, are given under the condition of incomplete compensation according to circuit theory. The influence of compensation capacitance errors on the output characteristics of the system is then analyzed. The Taylor expansions of the theoretical formulas are carried out to simplify the formulas. The influence degrees of compensation capacitance errors on the output characteristics are calculated according to the simplified formulas. The reasonable error ranges of the compensation capacitances are then determined according to the requirements of the output characteristics of the system in the system design. Finally, the validity of the theoretical analysis and the simplified processing is verified through experiments. The proposed method has a certain guiding role for practical engineering design, especially in mass production.

**Keywords:** wireless power transfer (WPT) system; series-series (SS) topology; compensation errors

## 1. Introduction

Inductively coupled wireless power transfer system utilizes time varying electromagnetic fields to transfer energy. It has been widely used in traffic, consumer electronics, underwater, mining equipment, and so on. Compared to the traditional plug-in power supply system, the wireless power transfer (WPT) system can achieve mechanical and electrical isolation, minimize cable and socket applications, and ensure safe operation in harsh environments [1,2]. Especially in electric bus and energy storage tram charging, the WPT primary side coil winding can be buried under the existing platform, and achieve station charging. In this manner, the battery capacity and charging time of the tram and bus will be reduced [3,4].

The WPT transfer coil is loosely coupled, thus resonance network is required to reduce the reactive power and improve system efficiency. The resonant network, also known as the compensation network, typically resonates with the inductance of the transfer coil, thereby enhancing the transfer efficiency and changing the input and output characteristics. At present, the basic compensation topologies are mainly composed of four types: series-series (SS), series-parallel (SP), parallel-series (PS), and parallel-parallel (PP) [5], while some more complex compensation topologies are derived on the basis of these four. The hybrid topology on the primary side is proposed in [6], and can switch between two basic compensation networks to satisfy the constant voltage (CV) and constant current (CC) modes for stationary electric vehicle (EV) charging. In [7–9], it is pointed out that LCL type topology can allow the current of the transmitting coil to present a constant current source characteristic, and is suitable

for the case of multi-load transfer. In [10], an LCC resonant network is proposed to adjust the current on the transmitting coil by selecting the capacitor value in series, so that the output characteristics of the constant voltage source can be obtained at the second side. In [11], a compensation network calculation method is presented to realize the constant voltage or constant current output of the second side under the condition that the coil parameters are determined. In [12], an S/SP constant voltage gain compensation topology is proposed, and, under full compensation, the voltage gain is independent of mutual inductance. In addition to the output characteristics of resonant networks, some scholars have performed research on the primary capacitance [13,14], input impedance [15], soft switching [16,17], the system transfer efficiency optimization method [18,19], and the image impedance matching method [20–22]. However, most of the above studies did not consider the influence of compensation errors. In practical application, the resonance network is difficult to compensate for perfectly and its good output characteristics may not be as well, as a result, due to the challenge in accurately measuring the mutual inductance and self-inductance of coils, the existence of stray capacitance of the coils, errors of the compensation capacitances, and aging of the compensation capacitors. According the circuit theory, reactive power is present in a system with imperfect compensation. The existence of reactive power increases the stress of the device, and affects the output characteristics of the WPT system. Although there are many ways to improve the compensation accuracy, such as measuring the system's self-inductance and other parameters as accurately as possible and using high-accuracy capacitors, the cost will raise, especially in mass production. Therefore, it is necessary to study how incomplete compensation affects the output characteristics and how much it affects for the determination of compensation accuracy in the system design.

This paper takes SS topology as an example, and simplifying the causes of incomplete compensation as the accuracy errors of the compensation capacitances. First, according to the circuit equations, the formulas for calculating the power factor and output power, and so on, of the system under incomplete compensation are listed. The changes of output characteristics of the system, such as power factor, output power, coil transfer efficiency, and capacitors' voltage stress, when the compensation capacitances are in error are analyzed in detail. Although [20] provides a method to recover both the reactive parts and values of the resistive parts of the load/source impedances, the calculation of the power factor, output power, and other indicators is still rather complex and cumbersome. In view of this situation, as the errors of the compensation capacitors are generally controlled within a relatively small range, the Taylor formula is used to expand the original formulas, so that the simplified formulas can intuitively reflect the influence of the parameters and the errors of the capacitors. In the system design, according to the requirements on output characteristics of the system, the capacitances' allowable error ranges that can meet the requirements are obtained, which provides the basis for the selection of reasonable capacitance accuracy.

## 2. Analysis of SS Compensation Topology

A typical schematic diagram of a WPT system with SS topology is shown in Figure 1.

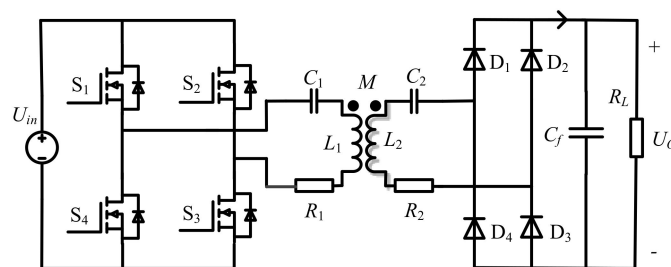


**Figure 1.** Typical structure of wireless power transfer (WPT) system with series-series (SS) compensation topology.

To simplify the analysis, Figure 1 can be equivalent to a simple model as shown in Figure 2. Among them,  $U_{in}$  and  $U_O$  is the input and output direct current (DC) voltage,  $U_1$  and  $U_2$  are the root-mean-square (RMS) values of the output voltage of the high frequency inverter and input voltage of the diode rectifier filter circuit,  $I_1$  and  $I_2$  are the RMS values of the output current of the high frequency inverter and input current of the diode rectifier filter circuit. By the Fourier decomposition, only the fundamental harmonic is considered, because high-order harmonic amplitudes are small and these harmonics can hardly be transmitted.  $L_1$  and  $L_2$  are the self-inductances of the loosely coupled transformer, and  $M$  is the coil mutual inductance.  $R_1$  and  $R_2$  are the internal resistances of the primary coil and secondary coil, and  $R_L$  and  $R_E$  are the load resistance and equivalent resistance, respectively.

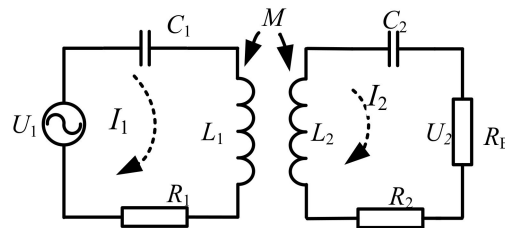


Figure 2. SS compensation topology equivalent circuit diagram.

By the Fourier decomposition of the square wave,  $U_1$  and  $U_2$  are expressed as:

$$U_1 = \frac{2\sqrt{2}}{\pi} U_{in} \quad (1)$$

$$U_2 = \frac{2\sqrt{2}}{\pi} U_O \quad (2)$$

According to Kirchhoff's Voltage Law (KVL), the following equations can be obtained:

$$\begin{cases} U_1 = Z_1 I_1 - j\omega M I_2 \\ -j\omega M I_1 + (Z_2 + R_E) I_2 = 0 \end{cases} \quad (3)$$

Among them:

$$\begin{cases} Z_1 = j\omega L_1 + \frac{1}{j\omega C_1} + R_1 \\ Z_2 = j\omega L_2 + \frac{1}{j\omega C_2} + R_2 \end{cases} \quad (4)$$

The relationship between the output equivalent resistance of coupling coils ( $R_E$ ) and load resistance ( $R_L$ ) is expressed as follows [23]:

$$R_E = \frac{8}{\pi^2} R_L + \frac{4\sqrt{2}}{\pi} \frac{V_{Dth}}{I_2} + 2r_D \quad (5)$$

where  $V_{Dth}$  is the threshold voltage, which has a constant value, and  $r_D$  is the equivalent resistance of the diode. And the loss on the diodes is usually ignored in the theoretical analysis, so  $R_E = \frac{8}{\pi^2} R_L$  is considered in the following.

The input current  $I_1$  and output current  $I_2$  can be calculated:

$$\begin{aligned} I_1 &= \frac{U_1(R_E + Z_2)}{\omega^2 M^2 + Z_1(R_E + Z_2)} \\ I_2 &= \frac{j\omega M U_1}{\omega^2 M^2 + Z_1(R_E + Z_2)} \end{aligned} \quad (6)$$

Next the input impedance of the primary side is obtained:

$$Z_{IN} = \frac{U_1}{I_1} = Z_1 + \frac{\omega^2 M^2}{R_E + Z_2} \quad (7)$$

The  $\omega$  is the operating angular frequency:

$$\omega = \frac{1}{\sqrt{L_1 C_1}} = \frac{1}{\sqrt{L_2 C_2}} \quad (8)$$

When the operating angular frequency meets Equation (8), the system is fully compensated and the primary input impedance  $Z_{IN}$  is pure resistive. Keeping the secondary under resonance can enhance the power transfer capability and efficiency, while keeping the primary under resonance can decrease the voltage-ampere (VA) rating of the source under the same output power [18]. It can be seen from Equation (8) that, when the coil self-inductance and system operating frequency are determined, the values of the compensation capacitors are only related to the operating frequency and self-inductance of the coils, and not to the load resistance and mutual inductance between the coils.

Power factor is an important index by which to measure the effect of power transfer, and is defined as the resulting phase between the voltage and current waveforms.

$$\lambda = \cos(-\theta_{Z_{IN}}) = \frac{\text{Re}[Z_{IN}]}{|Z_{IN}|} \quad (9)$$

$\theta_{Z_{IN}}$  is the input impedance angle of the primary, and  $\text{Re}[Z_{IN}]$  represents the real part of the input impedance. When the system is fully compensated, then  $\theta_{Z_{IN}} = 0^\circ$ , and  $\lambda = 1$ .

Next the output power is obtained:

$$P_o = |I_2|^2 R_E = \frac{\omega^2 M^2 U_1^2 R_E}{|\omega^2 M^2 + Z_1(R_E + Z_2)|^2} \quad (10)$$

The coil transfer efficiency can be expressed as follows:

$$\begin{aligned} \eta &= \frac{|I_2|^2 R_E}{|I_2|^2 R_E + |I_2|^2 R_2 + |I_1|^2 R_1} \\ &= \frac{\omega^2 M^2 R_E}{\omega^2 M^2 (R_E + R_2) + R_1 |R_E + Z_2|^2} \end{aligned} \quad (11)$$

The voltage stress of the compensation capacitor is:

$$U_{C_1} = \frac{|I_1|}{\omega C_1} \quad (12)$$

$$U_{C_2} = \frac{|I_2|}{\omega C_2} \quad (13)$$

### 3. Analysis of Influence of Compensation Errors

In practical application, due to the fact that the coils' parameters are difficult to measure accurately, the capacitors themselves contain errors, for which it is very difficult to perfectly compensate. Therefore, it is necessary to study the influence of incomplete compensation on the output characteristics of the system, then provide the basis for the selection of the capacitances' accuracy in the system design.

The accurate values of the compensation capacitances, calculated by Equation (8), are expressed by  $C_{10}$  and  $C_{20}$ , while the actual values of the compensation capacitances are expressed by  $C_1$  and  $C_2$ , and the ratio between the actual values and exact values the compensation capacitors are represented by  $k_1$  and  $k_2$ , thus  $C_1 = k_1 C_{10}$  and  $C_2 = k_2 C_{20}$  are given.

### 3.1. Influence on Power Factor

According to Equation (9), the power factor under incomplete compensation can be expressed as follows:

$$\lambda = \frac{\left(\omega^2 L_2^2 \left(\frac{k_2-1}{k_2}\right)^2 R_1 + (R_2 + R_E)(\omega^2 M^2 + R_1(R_2 + R_E))\right)}{\sqrt{\left(R_1 + \frac{\omega^2 M^2 (R_2 + R_E)}{\omega^2 L_2^2 \left(\frac{k_2-1}{k_2}\right)^2 + (R_2 + R_E)^2}\right)^2 + \omega^2 \left(\left(\frac{k_1-1}{k_1}\right) L_1 - \frac{\frac{k_2-1}{k_2} \omega^2 M^2 L_2}{\omega^2 L_2^2 \left(\frac{k_2-1}{k_2}\right)^2 + (R_2 + R_E)^2}\right)^2}} \quad (14)$$

It can be seen from Equation (14) that the calculation formula of the power factor without any treatment is rather complex. It is difficult to see the influence degree of the errors of two compensation capacitors on the power factor of the system. Therefore, next the above formula is dealt with as follows. The following two variables,  $e_1$  and  $e_2$ , are defined as follows:

$$\begin{aligned} e_1 &= \frac{k_1-1}{k_1} \\ e_2 &= \frac{k_2-1}{k_2} \end{aligned} \quad (15)$$

Clearly,  $e_1$  and  $e_2$  can be considered as the relative errors of the two capacitors. Then Equation (14) can be simplified as follows:

$$\lambda = \frac{\omega^2 L_2^2 e_2^2 R_1 + (R_2 + R_E)(\omega^2 M^2 + R_1(R_2 + R_E))}{(\omega^2 L_2^2 e_2^2 + (R_2 + R_E)^2) \sqrt{R_1^2 + \omega^2 e_1^2 L_1^2 + \frac{\omega^2 M^2 (\omega^2 M^2 - 2\omega^2 e_1 e_2 L_1 L_2 + 2R_1(R_2 + R_E))}{\omega^2 L_2^2 e_2^2 + (R_2 + R_E)^2}}} \quad (16)$$

Next, it can be seen from Equation (15) that when the errors of compensation capacitors are within a relatively small range, for example,  $\pm 10\%$  and  $\pm 5\%$ ,  $e_1$  and  $e_2$  are both real values close to zero, so that the Taylor formula can be used to expand Equation (16) at  $e_1 = 0$  and  $e_2 = 0$ , and the result is as follows:

$$\begin{aligned} \lambda &= 1 - \frac{\omega^6 L_2^2 M^4 e_2^2}{2(R_2 + R_E)^2 (\omega^2 M^2 + R_1(R_2 + R_E))^2} + O[e_2]^3 \\ &+ \left( \frac{\omega^4 M^2 L_1 L_2 e_2}{(\omega^2 M^2 + R_1(R_2 + R_E))^2} + O[e_2]^3 \right) e_1 \\ &+ \left( -\frac{\omega^2 L_1^2 (R_2 + R_E)^2}{2(\omega^2 M^2 + R_1(R_2 + R_E))^2} \right. \\ &+ \left. \frac{(-4L_1^2 L_2^2 R_1 \omega^6 M^2 (R_2 + R_E) + 5L_1^2 L_2^2 \omega^8 M^4) e_2^2}{4(\omega^2 M^2 + R_1(R_2 + R_E))^4} + O[e_2]^3 \right) e_1^2 \\ &+ O[e_1]^3 \end{aligned} \quad (17)$$

Ignoring the higher order terms, Equation (17) can be further simplified into:

$$\lambda = 1 - \frac{1}{2} \left( \frac{\omega^3 M^2 L_2 e_2 - \omega L_1 (R_2 + R_E)^2 e_1}{(\omega^2 M^2 + R_1(R_2 + R_E))(R_2 + R_E)} \right)^2 \quad (18)$$

In the actual system, the following formula should be satisfied:

$$R_E, \omega^2 M^2 \gg R_1, R_2 \quad (19)$$

When the coils internal resistances are neglected, the simplified formula of the power factor can be obtained:

$$\lambda \approx 1 - \frac{1}{2} \left( \frac{\omega L_2 e_2}{R_E} - \frac{L_2 R_E e_1}{\omega M^2} \right)^2 \quad (20)$$

It can be seen from Equation (20) that  $\omega$ ,  $L_1$ ,  $L_2$ ,  $M$ ,  $R_E$ ,  $e_1$  and  $e_2$  are all important factors which affect the power factor. Once the system is determined, there will be an optimal load calculated by Equation (21), in which the maximum coil transfer efficiency is obtained:

$$R_{E-max} = \sqrt{\frac{R_2(\omega^2 M^2 + R_1 R_2)}{R_1}} \quad (21)$$

Therefore, the errors of the capacitances will have a permissible range within which the power factor can still remain high.

### 3.2. Influence on Output Power

In the same manner, the influence of the capacitance errors on the output power can be explored. When errors exist, the output power is as follows:

$$P_o = \frac{\omega^2 M^2 R_E U_1^2}{\omega^2 (e_2 L_2 R_1 + e_1 L_1 (R_2 + R_E))^2 + (\omega^2 M^2 - \omega^2 e_1 e_2 L_1 L_2 + R_1 (R_2 + R_E))^2} \quad (22)$$

The simplified formula can be obtained as follows, by expanding Equation (22) with the Taylor formula, and ignoring the higher order terms:

$$P_o \approx \frac{\omega^2 M^2 R_E U_1^2}{(\omega^2 M^2 + R_1 (R_2 + R_E))^2} \left( 1 + \left( \frac{\omega L_2 e_2}{R_E} \right)^2 - \left( \frac{\omega L_2 e_2}{R_E} - \frac{L_1 R_E e_1}{\omega M^2} \right)^2 \right) \quad (23)$$

Thus the change rate of output power is:

$$\frac{\Delta P_o}{P_o} \approx \left( \frac{\omega L_2 e_2}{R_E} \right)^2 - \left( \frac{\omega L_2 e_2}{R_E} - \frac{L_1 R_E e_1}{\omega M^2} \right)^2 \quad (24)$$

### 3.3. Influence on Coil Transfer Efficiency

When the capacitances are in error, the coil transfer efficiency is calculated as follows:

$$\begin{aligned} \eta &= \frac{\omega^2 M^2 R_E}{\omega^2 M^2 (R_E + R_2) + R_1 ((R_E + R_2)^2 + \omega^2 L_2^2 e_2^2)} \\ &= \frac{1}{1 + \frac{R_2}{R_E} + \frac{L_2^2 R_1}{M^2 R_E} e_2^2 + \frac{(R_E + R_2)^2 R_1}{\omega^2 M^2 R_E}} \end{aligned} \quad (25)$$

Clearly, it can be seen from Equation (25) that, the original formula itself is simple enough, so there is no need to use the Taylor formula to expand it, and the error of the primary series capacitor does not affect the transfer efficiency, only the error of the secondary series capacitor does.

### 3.4. Influence on Capacitors Voltage Stress

In general, when there are errors in the compensation capacitors, the current in the coils will change, as will the capacitors' voltage stress. Thus, it is necessary to study the influence of the capacitance errors on the capacitors voltage stress for the actual selection of voltage stress class of the compensation capacitors.

When the two compensation capacitors both contain errors, the voltage stress of  $C_1$  is as follows:

$$\begin{aligned} U_{C_1} &= \frac{\omega L_1 (1 - e_1) \sqrt{\omega^2 L_2^2 e_2^2 + (R_2 + R_E)^2} U_1}{\sqrt{\omega^2 (e_2 L_2 R_1 + e_1 L_1 (R_2 + R_E))^2 + (\omega^2 M^2 - \omega^2 e_1 e_2 L_1 L_2 + R_1 (R_2 + R_E))^2}} \\ &= \frac{\omega L_1 (R_2 + R_E) U_1}{\omega^2 M^2 + R_1 (R_2 + R_E)} \left( 1 - e_1 + \left( \frac{\omega L_2 e_2}{R_E} \right)^2 - \frac{1}{2} \left( \frac{\omega L_2 e_2}{R_E} - \frac{L_1 R_E e_1}{\omega M^2} \right)^2 \right) \end{aligned} \quad (26)$$

Clearly, the change rate of voltage stress of  $C_1$  is:

$$\frac{\Delta U_{C_1}}{U_{C_1}} = -e_1 + \left(\frac{\omega L_2 e_2}{R_E}\right)^2 - \frac{1}{2} \left(\frac{\omega L_2 e_2}{R_E} - \frac{L_1 R_E e_1}{\omega M^2}\right)^2 \tag{27}$$

And the voltage stress of  $C_2$  is:

$$U_{C_2} = \frac{\omega^2 M(1-e_2)L_2 U_1}{\sqrt{\omega^2(e_2 L_2 R_1 + e_1 L_1(R_2 + R_E))^2 + (\omega^2 M^2 - \omega^2 e_1 e_2 L_1 L_2 + R_1(R_2 + R_E))^2}} \tag{28}$$

$$= \frac{\omega^2 M L_2 U_1}{\omega^2 M^2 + R_1(R_2 + R_E)} (1 - e_2) \left(1 - \frac{1}{2} \left(\frac{\omega L_2 e_2}{R_E}\right)^2 + \frac{1}{2} \left(\frac{\omega L_2 e_2}{R_E} - \frac{L_1 R_E e_1}{\omega M^2}\right)^2\right)$$

The change rate of voltage stress of  $C_2$  is:

$$\frac{\Delta U_{C_2}}{U_{C_2}} = (1 - e_2) \left(1 - \frac{1}{2} \left(\frac{\omega L_2 e_2}{R_E}\right)^2 + \frac{1}{2} \left(\frac{\omega L_2 e_2}{R_E} - \frac{L_1 R_E e_1}{\omega M^2}\right)^2\right) - 1 \tag{29}$$

Therefore, the change rates of voltage stress of  $C_1$  and  $C_2$  can be calculated using Equations (27) and (29) when there are errors in the compensation capacitances, which is important for determining the voltage stress class of the compensation capacitors.

#### 4. System Performance Analysis

According to the parameters of the actual coils, taking the capacitor precision of  $\pm 10\%$  as an example, the power factor, output power, and coil transfer efficiency varying with the capacitance errors are shown in Figure 3 using the parameters shown in Table 1.

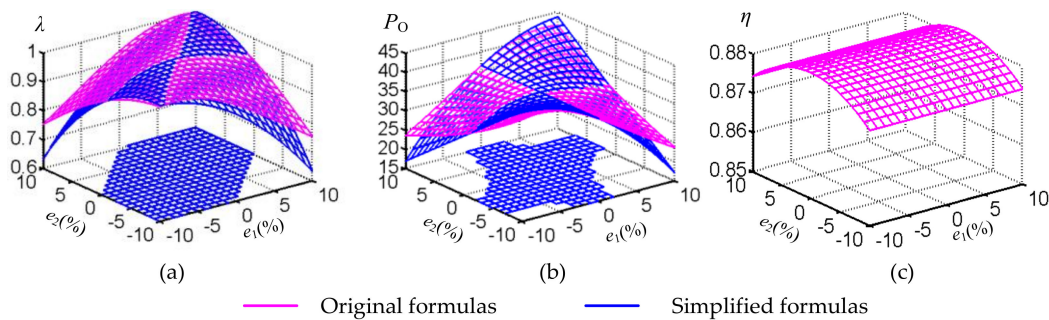


**Figure 3.** The variation of output characteristics with capacitance errors calculated using the original and simplified formulas, and allowable capacitance error ranges calculated using the simplified formulas: (a) The power factor varying with capacitance errors and allowable capacitance error range when the power factor is greater than 0.9; (b) The output power varying with capacitance errors and allowable capacitance error range when the output power change rate is smaller than 0.1; (c) The coil transfer efficiency varying with capacitance errors.

**Table 1.** System parameters.

| Parameter                                    | Value |
|--|-------|
| Resonant frequency $f$ (KHz)                 | 21.9  |
| Inverter output voltage $U_1$ (V)            | 8.0   |
| Primary coil inductance $L_1$ ( $\mu$ H)     | 47.1  |
| Primary coil resistance $R_1$ ( $\Omega$ )   | 0.09  |
| Secondary coil inductance $L_2$ ( $\mu$ H)   | 45.7  |
| Secondary coil resistance $R_2$ ( $\Omega$ ) | 0.12  |
| Mutual inductance $M$ ( $\mu$ H)             | 10.6  |
| Equivalent resistance $R_E$ ( $\Omega$ )     | 1.4   |

As shown in Figure 3a, the power factor remains high when the errors are within a certain range. Taking the power factor of no less than 0.9 as an example, the allowable range of capacitance errors calculated using the simplified formula is drawn, as shown in the shaded area of the XOY plane in Figure 3a. In some areas, such as in the vicinity of  $e_1 = 10\%$  and  $e_2 = -10\%$ , the error between the original and simplified formula is larger than 10%, but the power factor in these regions is low, which will be abandoned. And the error between the original and simplified formula is smaller than 4% when the capacitance errors are within the allowable range calculated using the simplified formula. Thus, it is acceptable to use the Taylor formula to expand the original formula and simplify it. Besides, it can be seen from Figure 3a that, when two compensation capacitances are both larger and smaller than the exact values, the power factor remains high. The reason is that when the compensation capacitance of the secondary is larger (smaller), the secondary is in a capacitive (inductive) state, that is, the imaginary part of  $Z_2$  is negative (positive), while the reflection impedance reflected to the primary is inductive (capacitive), that is, the imaginary part of  $\left(\frac{\omega^2 M^2}{R_E + Z_2}\right)$  is positive (negative), as shown in Equation (7). Therefore, the equivalent load of the inverter may be turned into pure resistance if the compensation capacitance of the primary is larger (smaller) too, and the high power factor is maintained as a result.

As shown in Figure 3b, the output power of the system is significantly affected by the capacitance errors when the parameters shown in Table 1 are employed. When the change rate of the output power of the system is limited to no more than 10%, the allowable error range of the compensation capacitance is shown as the shaded area of the XOY plane in Figure 3b. The error between the original and simplified formula is smaller than 5% when the capacitance errors are within the allowable range calculated using the simplified formula. So, similarly, the large error in some regions does not affect the final result.

Combined with Figure 3c and the theoretical calculation formula above, the error of the primary series capacitor does not affect the coil transfer efficiency. Only the error of the secondary series compensation capacitor affects it, and the existence of the error reduces the coil transfer efficiency. When the error of the secondary series compensation capacitor is 10%, the coil transfer efficiency is reduced from 88.2% to 87.4%, which indicates that the coil transfer efficiency is less affected by the error of the secondary series compensation capacitor when the system parameters shown in Table 1 are employed. Thus, the effect of capacitance errors on coil transfer efficiency is ignored when calculating the allowable capacitance error range.

The variation of the voltage stress of the primary series capacitor and secondary series capacitor are shown in Figure 4a,b. When there are errors in the compensation capacitors, the system will generate reactive power, thereby affecting the current amplitude and the voltage amplitude of the capacitors. In practical use, the withstand voltage level of capacitors is also a factor that cannot be ignored, as it affects the system safety. Therefore, it is necessary to restrict the voltage stress of the compensation capacitors. When the rise rates of the voltage stress of capacitors are limited to no more than 10%, the allowable error ranges of the compensation capacitance are shown as the shaded area of the XOY plane in Figure 4a,b.

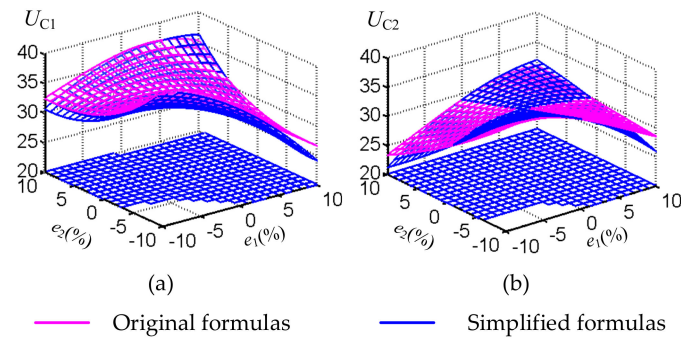


**Figure 4.** The variation of the capacitors voltage stress with capacitance errors calculated using the original and simplified formulas, and allowable capacitance error ranges calculated using the simplified formulas: **(a)** The voltage stress of  $C_1$  varying with capacitance errors and allowable capacitance error range when the rise rate of the voltage stress of  $C_1$  is smaller than 0.1; **(b)** The voltage stress of  $C_2$  varying with capacitance errors and allowable capacitance error range when the rise rate of the voltage stress of  $C_2$  is smaller than 0.1.

The selection of the accuracy of compensation capacitors should meet the restrictions of the system on power factor, output power, capacitors voltage stress, and other targets. Therefore, in actual use, it is necessary to take the intersection of the shaded area on the XOY plane shown in Figures 3 and 4. The allowable error ranges of the compensation capacitances are shown in Figure 5. The blue and yellow regions are the allowable capacitance error ranges meeting the requirements of power factor and output power, respectively. And the green and cyan regions, which is sheltered, are the allowable capacitance error ranges meeting the requirements of the voltage stress of  $C_1$  and  $C_2$ , respectively. The red region is the intersection of all the above allowable range.

In practical application, the selection of two compensation capacitors is independent. Therefore, some areas, where the accuracy requirement of a capacitor is related to another's, for instance, when  $e_1 = 10\%$ ,  $e_2$  must be between 3% and 7%, are abandoned. And it can be seen from the red area,  $e_1 = \pm 3\%$ ,  $e_2 = \pm 7\%$ , and  $e_1 = \pm 4\%$ ,  $e_2 = \pm 5\%$  and other selections are all acceptable. Obviously, the price of a capacitor rises sharply with the increase of precision. Therefore,  $e_1 = \pm 4\%$ ,  $e_2 = \pm 5\%$  may a better choice, finally, just like the purple region shows.

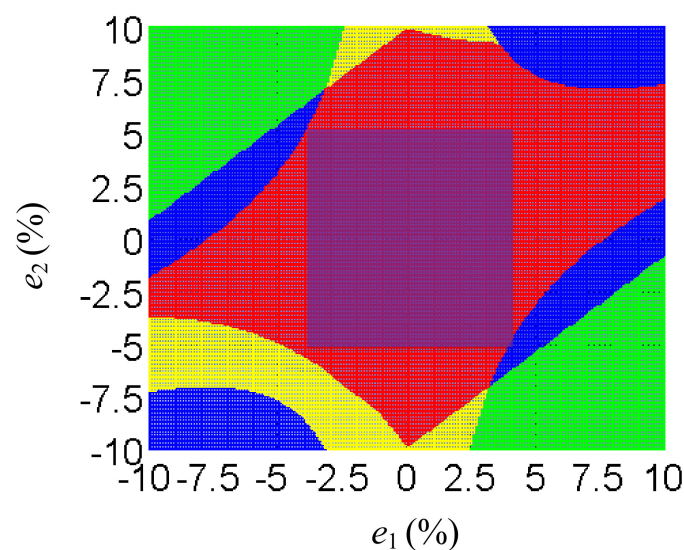


**Figure 5.** Intersection of allowable capacitance errors satisfying the system requirements on the output characteristics.

## 5. Experimental Verification

Experimental verification is performed using the experimental platform, as shown in Figure 6. This platform adopts a TMS320F28335 DSP (TI, Dallas, TX, USA) as the control core and the primary side inverter switch is an FMP65N15T2 (Fuji, Japan), a MOSFET produced by Fuji Electric. The primary and secondary inductors are square coils with a single layer and a turn number of 12, composed of tightly-wound litz wires with a diameter of 3 mm. The length and width of square coils are 25 cm and 18 cm, respectively, and the gap between the primary and secondary is 6.5 cm. The input voltage  $U_1$  and output voltage  $U_2$  are measured using a THDP0200 (Tektronix, OH, USA), and the input current  $I_1$  and output current  $I_2$  are measured using a TCP0030A (Tektronix, OH, USA). The phase between the voltage and current waveforms are measured using the phase measurement function of a Tektronix dpo3034 digital phosphor oscilloscope (Tektronix, OH, USA), and the other data are calculated using the measured output voltage and current of the inverter and load. And the system uses the parameters listed in Table 1 for experimental verification. The actual capacitance values, the mutual inductance, and the self-inductance of coils are measured by a HM8118 LCR bridge (HAMEG, Mainhausen, Germany), and the actual capacitance values of  $C_1$  and  $C_2$  and the calculated values of  $e_1$  and  $e_2$  are listed in Table 2.

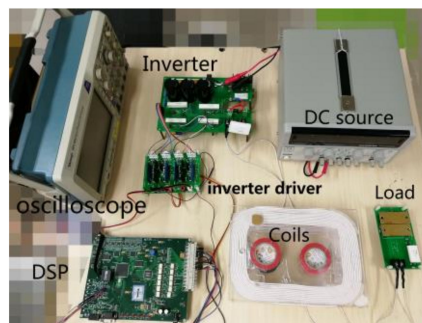


Figure 6. Experimental platform device.

Table 2. Capacitance parameters.

| Parameter | Value               | Value               | Value               | Value               | Value               |
|-----------|---------------------|---------------------|---------------------|---------------------|---------------------|
| $C_1$     | 1.014 $\mu\text{F}$ | 1.059 $\mu\text{F}$ | 1.113 $\mu\text{F}$ | 1.171 $\mu\text{F}$ | 1.235 $\mu\text{F}$ |
| $e_1$     | −10.1%              | −5.2%               | −0.3%               | +4.8%               | +9.8%               |
| $C_2$     | 1.045 $\mu\text{F}$ | 1.090 $\mu\text{F}$ | 1.145 $\mu\text{F}$ | 1.202 $\mu\text{F}$ | 1.279 $\mu\text{F}$ |
| $e_2$     | −10.0%              | −5.3%               | +0.3%               | +4.4%               | +10.2%              |

According to the actual capacitance values, the calculated values of  $e_1$  are −10.1%, −5.2%, −0.3%, +4.8%, and +9.8%, respectively, while those of  $e_2$  are −10.0%, −5.3%, +0.3%, +4.4%, and +10.2%. These capacitors are employed, respectively, thus 25 sets of experiments are carried out. When the experiment is carried out, and there is no rectifier in the secondary. Limited by the parameters of the coils, the power level of the confirmatory experiment is very small, only a few dozen watts. And it can be seen from Equation (5) that, the equivalent resistance of coupling coils  $R_E$  can be considered to be equal to  $\frac{8}{\pi^2} R_L$  only when  $\left(\frac{4\sqrt{2}}{\pi} \frac{V_{Dth}}{I_2} + 2r_D\right)$  is smaller than  $\frac{8}{\pi^2} R_L$  and can be ignored, and the loss on the rectifier diodes will not significantly affect the system's output characteristics. When there is a rectifier in the secondary, the output voltage  $U_2$  will be a square wave due to the existence of the filter capacitance, which is a sinusoidal wave when there is no rectifier. But high-order harmonic amplitudes are small and these harmonics can hardly be transmitted. So it is feasible to use the resistor without parasitic inductance to be connected to the compensated coil in the experiment. And the output voltage and current waveforms of the inverter and load under the different compensation capacitance errors are shown in Figure 7, in which the annotation  $U_1$  is the RMS value of the fundamental harmonic of the inverter's output voltage.

The power factor, output power, and coil transfer efficiency and capacitors' voltage stress varying with the capacitance errors obtained in the experiments are shown in Figure 8, in which the data of the magenta points are the calculated results using the measured output voltage and the current of the inverter and load. It can be seen from the experimental results that the power factor, output power, transfer efficiency, and the capacitors' voltage stress change slowly as the capacitance errors change, thus, the experimental data can be fitted by MATLAB software. The approximate data of the power factor, output power, coil transfer efficiency, and the capacitors' voltage stress as the capacitance error changes when the capacitance error is within 10% can be obtained, as shown in Figure 8.

By comparing Figure 8 with the calculated results of Section 3, it can be seen that the variation trend of the power factor, output power, coil transfer efficiency, and the capacitors' voltage stress with capacitance errors is in line with the theoretical calculation results. And the error between the experimental results and theoretical calculation is less than 10%.

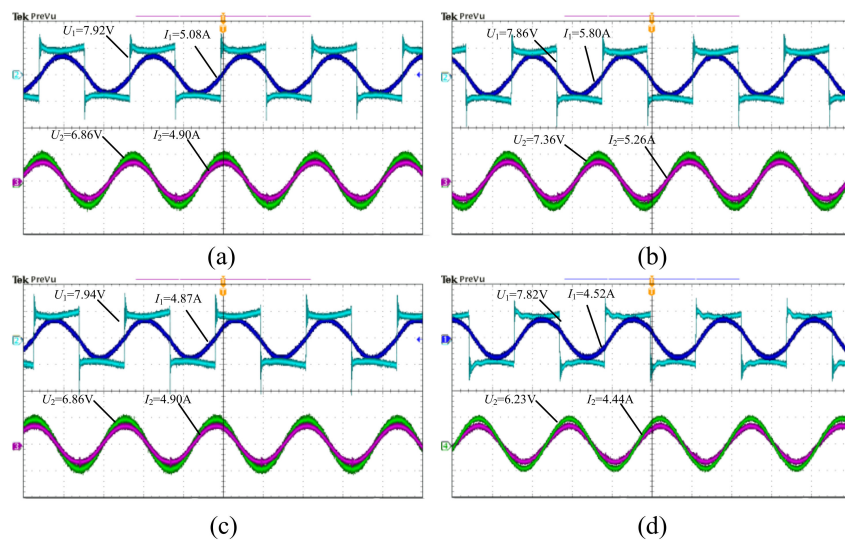


**Figure 7.** Experiment waveforms: (a)  $e_1 = -0.3\%$ ,  $e_2 = +0.3\%$ ; (b)  $e_1 = -10.1\%$ ,  $e_2 = -10.0\%$ ; (c)  $e_1 = -5.2\%$ ,  $e_2 = +0.3\%$ ; and (d)  $e_1 = +9.8\%$ ,  $e_2 = +4.4\%$ .

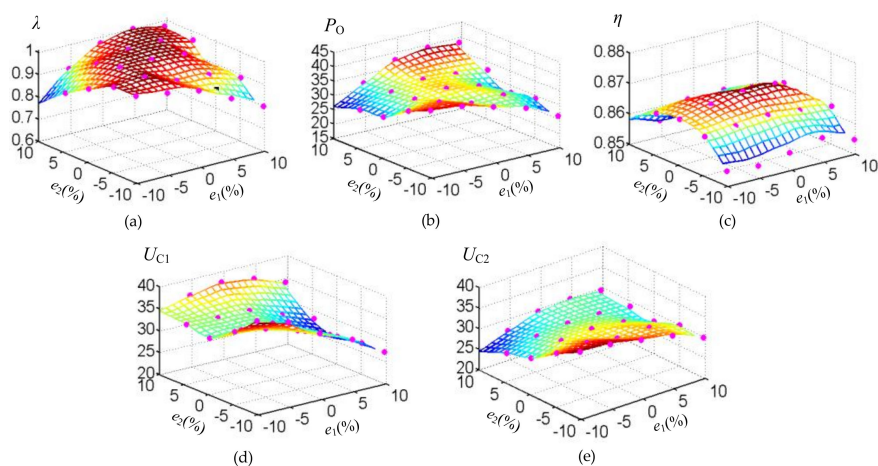


**Figure 8.** The variation of output characteristics with capacitance errors and the variation of output characteristics fitted by the experimental data: (a) The power factor varying with capacitance errors; (b) the output power varying with capacitance errors; (c) The coil transfer efficiency varying with capacitance errors; (d) The voltage stress of  $C_1$  varying with capacitance errors; (e) The voltage stress of  $C_2$  varying with capacitance errors.

The analysis results show that error between the theory and experiment exists in many aspects. First, in the actual circuit, the equivalent load of the inverter, capacitive or inductive, will affect the turn-on and turn-off characteristics of the switches, and this is not considered in the theoretical calculation. When the input DC voltage of the inverter is constant, 10 V in this experiment, the RMS value of the output voltage of the inverter changes slightly with the load's capacitive or inductive state, as shown in Figure 7, which will further affect the output power and the capacitors' voltage stress. In addition, the dead time of the driving pulse of the inverter, approximate treatment in the theoretical calculation formulas, and actual electromagnetic leakage will all affect the transfer characteristics of the system, while these factors are not taken into consideration. Thus, although there is an error between the experimental results and theoretical calculations, the error is within an acceptable range, and the experiment can verify the validity of the theoretical analysis.

According to the requirements of the system on the power factor, output power change rate, and voltage stress rise rate of the capacitors assumed in Section 3, the capacitance error range which meets the above requirements in the actual experiment can be obtained. As shown in Figure 9, the blue area is the allowable capacitance error range of the experimental data, and the red area is the allowable range derived from theoretical calculation. In the upper right corner of Figure 9, the error between the experimental results and theoretical calculations is larger than other regions, this is because, in this area, the equivalent load of the inverter is capacitive, the RMS value of the fundamental harmonic of the inverter's output voltage is smaller than 8V in the experiments, resulting in output power, and the voltage stress is less than the theoretical value. When the compensation capacitance of the primary is larger, the equivalent load of the inverter may be turned into pure resistance if the compensation capacitance of the secondary is large, too, just as the analysis in Section 3 shows, and the output voltage of the inverter may be increased to 8 V again, therefore, the error comes out.

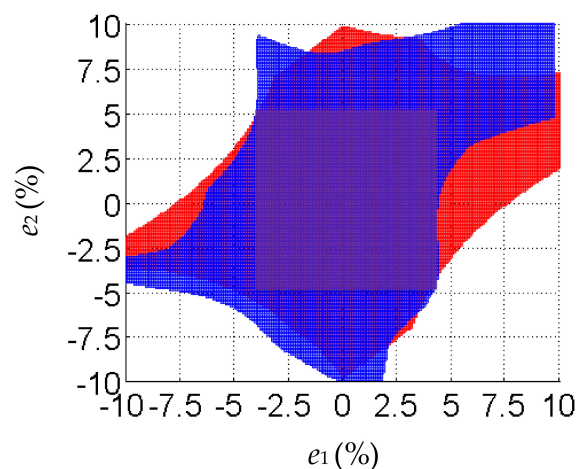


**Figure 9.** The calculated allowable range and experimental allowable range.

As shown in the figure above, as far as the allowable range satisfying the entire system's requirements is concerned, the error between the theoretical calculation and actual experiment is within the allowable range, thus proving the validity of the method.

## 6. Conclusions

This paper presents a method to determine the accuracy of compensation capacitance in practical engineering applications. The theoretical calculation formulas of the power factor, output power, coil transfer efficiency and capacitors' voltage stress of the WPT system with SS compensation topology are derived while the system is not completely compensated. The influence trend of capacitance errors on these characteristic indexes can be intuitively obtained after the Taylor formula is used to expand and simplify the original formulas, and these characteristic indexes can be calculated simply according

to the simplified formulas when the capacitance errors are known. A reasonable allowable range of capacitance errors,  $\pm 4\%$  of  $C_1$  and  $\pm 5\%$  of  $C_2$ , can be obtained according to the requirements of the system on the power factor, output power, and capacitors' voltage stress. Especially when the product with the WPT technology is mass-produced, the cost could go down. Thus, the proposed method has a certain guiding role in practical engineering applications.

**Acknowledgments:** Thanks for Fuji Electric Co., Ltd.'s support with the MOSFET devices.

**Author Contributions:** The main idea of this paper is proposed by Yi Wang and Fei Lin. Yi Wang wrote this paper. Zhongping Yang designed the experiments. Zhiyuan Liu performed the experiments.

**Conflicts of Interest:** The authors declare no conflict of interest.

## References

1. Shin, J.; Shin, S.; Kim, Y.; Ahn, S.; Lee, S.; Jung, G.; Jeon, S.J.; Cho, D.H. Design and implementation of shaped magnetic-resonance-based wireless power transfer system for roadway-powered moving electric vehicles. *IEEE Trans. Ind. Electron.* **2014**, *61*, 1179–1192. [[CrossRef](#)]
2. Yusop, Y.; Saat, S.; Nguang, S.K.; Husin, H.; Ghani, Z. Design of Capacitive Power Transfer Using a Class-E Resonant Inverter. *J. Power Electron.* **2016**, *16*, 1678–1688. [[CrossRef](#)]
3. Zhang, W.; Wong, S.C.; Tse, C.K.; Chen, Q. An optimized track length in roadway inductive power transfer systems. *IEEE J. Emerg. Sel. Top. Power Electron.* **2014**, *2*, 598–608. [[CrossRef](#)]
4. Covic, G.A.; Boys, J.T. Modern trends in inductive power transfer for transportation applications. *IEEE J. Emerg. Sel. Top. Power Electron.* **2013**, *1*, 28–41. [[CrossRef](#)]
5. Wang, C.S.; Stielau, O.H.; Covic, G.A. Design considerations for a contactless electric vehicle battery charger. *IEEE Trans. Ind. Electron.* **2005**, *52*, 1308–1314. [[CrossRef](#)]
6. Qu, X.; Han, H.; Wong, S.C.; Chi, K.T.; Chen, W. Hybrid IPT topologies with constant current or constant voltage output for battery charging applications. *IEEE Trans. Power Electron.* **2015**, *30*, 6329–6337. [[CrossRef](#)]
7. Kissin, M.L.G.; Huang, C.Y.; Covic, G.A.; Boys, J.T. Detection of the tuned point of a fixed-frequency LCL resonant power supply. *IEEE Trans. Power Electron.* **2009**, *24*, 1140–1143. [[CrossRef](#)]
8. Borage, M.; Tiwari, S.; Kotaiah, S. Analysis and design of an LCL-T resonant converter as a constant-current power supply. *IEEE Trans. Ind. Electron.* **2005**, *52*, 1547–1554. [[CrossRef](#)]
9. Wu, H.H.; Gilchrist, A.; Sealy, K.D.; Bronson, D. A high efficiency 5 kW inductive charger for EVs using dual side control. *IEEE Trans. Ind. Inform.* **2012**, *8*, 585–595. [[CrossRef](#)]
10. Geng, Y.; Yang, Z.; Lin, F.; Hu, S. A High Efficiency Charging Strategy for a Supercapacitor Using a Wireless Power Transfer System Based on Inductor/Capacitor/Capacitor (LCC) Compensation Topology. *Energies* **2017**, *10*, 135. [[CrossRef](#)]
11. Qu, X.; Jing, Y.; Han, H.; Wong, S.C. Higher Order Compensation for Inductive-Power-Transfer Converters with Constant-Voltage or Constant-Current Out-put Combating Transformer Parameter Constraints. *IEEE Trans. Power Electron.* **2017**, *32*, 394–405. [[CrossRef](#)]
12. Hou, J.; Chen, Q.; Wong, S.; Tse, C.K. Analysis and control of series/series-parallel compensated resonant converter for contactless power transfer. *IEEE J. Emerg. Sel. Top. Power Electron.* **2015**, *3*, 124–136.
13. Zhu, Q.; Wang, L.; Guo, Y.; Liao, C.; Li, F. Applying LCC compensation network to dynamic wireless EV charging system. *IEEE Trans. Ind. Electron.* **2016**, *63*, 6557–6567. [[CrossRef](#)]
14. Zhao, J.; Cai, T.; Duan, S.; Feng, H.; Chen, C.; Zhang, X. A general design method of primary compensation network for dynamic WPT system maintaining stable transmission power. *IEEE Trans. Power Electron.* **2016**, *31*, 8343–8358. [[CrossRef](#)]
15. Villa, J.L.; Sallan, J.; Osorio, J.F.S.; Llombart, A. High-misalignment tolerant compensation topology for ICPT systems. *IEEE Trans. Ind. Electron.* **2012**, *59*, 945–951. [[CrossRef](#)]
16. Lu, R.; Wang, T.; Mao, Y.; Zhu, C. Analysis and design of a wireless closed-loop ICPT system working at ZVS mode. In Proceedings of the 2010 IEEE Vehicle Power and Propulsion Conference (VPPC), Lille, France, 1–3 September 2010; pp. 1–5.
17. Tang, C.S.; Sun, Y.; Su, Y.G.; Nguang, S.K.; Hu, A.P. Determining Multiple Steady-State ZCS Operating Points of a Switch-Mode Contactless Power Transfer System. *IEEE Trans. Power Electron.* **2009**, *24*, 416–425. [[CrossRef](#)]

18. Zhang, Y.; Chen, K.; He, F.; Zhao, Z.; Lu, T.; Yuan, L. Closed-Form Oriented Modeling and Analysis of Wireless Power Transfer System with Constant-Voltage Source and Load. *IEEE Trans. Power Electron.* **2015**, *31*, 3472–3481. [[CrossRef](#)]
19. Tan, L.; Yan, C.; Huang, X.; Wang, W.; Chen, C. Stable Voltage Online Control Strategy of Wireless Power Transmission System. *Trans. China Electrotech. Soc.* **2015**, *30*, 12–17.
20. Roberts, S. Conjugate-Image Impedances. *Proc. IRE* **1946**, *34*, 198–204. [[CrossRef](#)]
21. Inagaki, N. Theory of image impedance matching for inductively coupled power transfer systems. *IEEE Trans. Microwav. Theory Tech.* **2014**, *62*, 901–908. [[CrossRef](#)]
22. Dionigi, M.; Mongiardo, M.; Perfetti, R. Rigorous network and full-wave electromagnetic modeling of wireless power transfer links. *IEEE Trans. Microwav. Theory Tech.* **2015**, *63*, 65–75. [[CrossRef](#)]
23. Matsumoto, H.; Shibako, Y.; Neba, Y. Contactless power transfer system for AGVs. *IEEE Trans. Ind. Electron.* **2018**, *65*, 251–260. [[CrossRef](#)]



© 2017 by the authors. Licensee MDPI, Basel, Switzerland. This article is an open access article distributed under the terms and conditions of the Creative Commons Attribution (CC BY) license (<http://creativecommons.org/licenses/by/4.0/>).